

Office of the Chief Scientist for Human Factors

Vertical Flight Human Factors

Program Review
FY04



Federal Aviation Administration
ATO-P R&D HF (Room 907A)
800 Independence Avenue, S.W.
Washington, D.C. 20591
phone (202) 267-8758
e-mail: william.krebs@faa.gov
<http://www.hf.faa.gov/krebs>

The Federal Aviation Administration Office of the Chief Scientific and Technical Advisor for Human Factors (ATO-P R&D HF) vertical flight human factors program is a relative new research domain. Research in this area is meant to identify specific human factors associated with helicopter flight regimes within the National Airspace System. Such issues include certification and regulation of civilian flights with night-vision-goggles devices, simultaneous non-interfering operations, and implications of tilt-rotor controls.

The following report summarizes projects between October 1st, 2003 and September 30th, 2004. These projects attempt to address requirements identified by the Federal Aviation Administration Flight Standards and Certification offices. The intent of this report is to allow Federal Aviation Administration sponsors to determine whether their requirements have been satisfactorily addressed, allow investigators to receive feedback from Federal Aviation Administration sponsors and other interested parties, and to provide feedback to the ATO-P R&D HF vertical flight human factors program manager on the quality of the research program. Basically, this document is a means of holding each group (sponsor, investigator, ATO-P R&D HF program manager) accountable to ensure that the program is successful.

The FY03 funded projects had \$250,000 contract dollars distributed to three projects.

Address questions or comments to:

William K. Krebs, Ph.D.

Vertical Flight Human Factors

FY04 Funded Projects

<u>Project Title</u>	<u>Page #</u>
Investigating ATC Procedures for Simultaneous Non-Interfering Flight Within the National Airspace System	1
Progress on Flight Video Data Analyses for Assessment of PVFR Routes and SNI Operations for Rotorcraft	6
Night Vision Imaging System Lighting Compatibility Assessment Methodology: Part 2	11

INVESTIGATING ATC PROCEDURES FOR SIMULTANEOUS NON-INTERFERING FLIGHT WITHIN THE NATIONAL AIRSPACE SYSTEM

Principal Investigators:
Dr. R. Darken, & CDR J. Sullivan USN
700 Dyer Rd. Code MOVES
Naval Postgraduate School
Monterey, California 93943-5001
831-656-7588
831-656-7599 (fax)

November 9, 2004

1. Purpose and Rationale

It is generally assumed that GPS utilization by helicopter pilots conducting simultaneous non-interfering routes will improve safety and enable more efficient use of national airspace system. However, there is a limited body of empirical evidence to validate this assumption and suggest training and operating procedures for realizing the full potential of GPS SNI routes. The ideal environment in which to explore GPS use on SNI routes would allow evaluators to manipulate variables that affect how pilots use GPS such as weather, navigation queue and traffic density. This test environment would also allow experimenters to make observations about GPS use and navigation performance without the expense and risk to flight crews and ground personnel associated with in-flight testing. Simulation has the potential to provides this. However, before simulation is assumed to be a valid medium for study, piloting procedures and navigation performance in real and simulated environments must be compared and verified.

This study attempts to help define optimal operating and training procedures for conducting SNI routes with GPS by studying pilot's scan patterns and navigation performance based on data collected in flight. Further, this study attempts to compare pilot scan patterns and navigation performance in real and simulated environments to determine if simulation is a viable framework for future study of helicopter pilot's use of GPS on SNI routes.

2. Study Framework

This experiment is divided into several separate phases. The initial phase involved constructing a route, refining data collection equipment and procedures and collecting in-flight data. The second phase of the experiment involved creating a virtual replica of the actual test environment. This phase will be completed later this year by replicating the in-flight experiment in the simulator and verifying the correlation of the data sets.

2.1. In-Flight Phase

2.1.1. Test aircraft

The OH-58 was selected as the test aircraft. This airframe met all of the requirements describe in the initial test plan. Of primary importance, the OH-58 is typical of the aircraft that use PVFR/SNI routes, it has a large experience pool from which to draw subjects, has avionics compatible with the mission, and can accommodate test equipment and personnel. The actual test aircraft is shown in Figure 1.



Figure 1. OH-58 test aircraft.

2.1.2. Test route

The test route was created in the airspace near Tullahoma Municipal Airport in eastern Tennessee. The route was designed to approximate actual SNI routes in terms of level of difficulty and salience of visual cues. In addition to this, the route was designed to have an even distribution of direction and magnitude of turns.

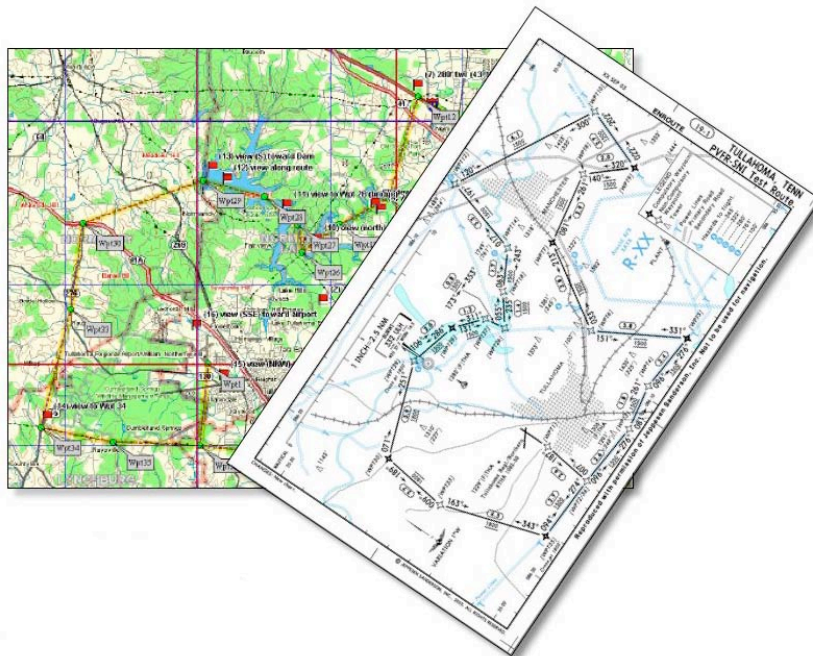


Figure 2. Test flight plan.

2.2. Virtual Flight Phase

2.2.1. Virtual Tullahoma

Creation of a virtual replica of Tullahoma required several major phases of development outlined below:

Image display device

The image display hardware system consists of three rear-projected screen and projector support structures arranged in a 'U' shape (see Figure 3). A mock cockpit is positioned on a raised platform facing the center screen. The system was designed around the physical constraints of the Training and Simulation Laboratory at NPS. Designed to occupy minimal floor space, it can be easily moved and reconfigured. The system is driven by three Christie LX3600 projectors equipped with short throw lenses. The projectors have a native resolution of 1024x768 pixels, output 3600 lumens and have a contrast uniformity ratio of 90%. The lens has a 0.8::1 throw-to-distance ratio, allowing the rear projection system to rely on a single mirror to produce sufficient image size while occupying minimal footprint. The systems' first-surface mirror reflects 96% of the incident light. Images are projected onto an IRUS projection screen. The screen is NTSC aspect ratio.



Figure 3. The apparatus for the simulator.

Visual, audio and data generation system

The visual, audio and data generation system is based on COTS (commercial off-the-shelf) personal computers and open source or COTS software. The system outlined in Figure 4 consists of two small form factor PCs and three COTS PCs. A single PC is used to read the flight controls and calculate the aircraft position and attitude using Laminar Research X-Plane flight simulator software. This position information is broadcast to a second, 'host' PC. This host PC acts as controller for the image and audio generation PCs. It also drives the cockpit gauges and outputs time and position information for data analysis. The three image-generation PCs receive aircraft position, attitude and other relevant simulation data from the host. These PCs render the out-the-window view based on their position relative to the operator. The host PC allows for full control of the simulation variables including loading databases, altering the view frustum

based on the angle between the screen and operator, and varying time of day and visibility.

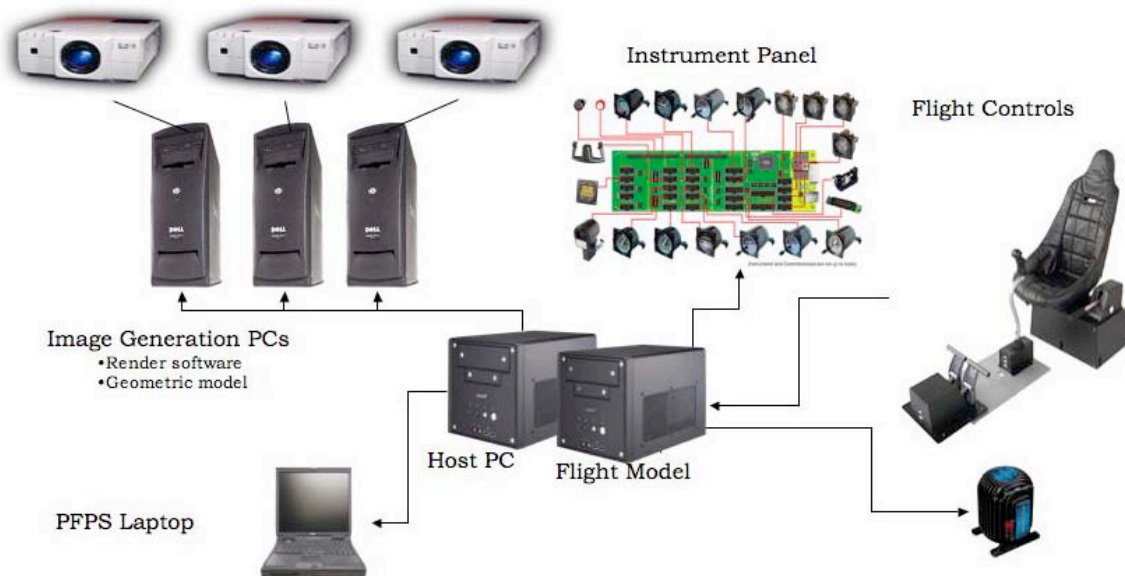


Figure 4. Schematic diagram of the apparatus for the simulator.

Cockpit replica

The cockpit replica consists of a seat, flight control system and cockpit gauges. The seat and flight control system (provided by Flight Link Incorporated) consists of a seat, cyclic, collective and rudder pedals. This system does not have a force trim system, nor is control loading using force feedback modeled. Initial usability studies suggest this system approximates the feel and workload sufficiently to perform en route navigation.

The instrument panel was based on the engineering diagrams for the OH-58. Physical gauges provided by SimKits populate the instrument panel. The gauges are fitted with faceplates that closely approximate the test aircraft. The gauges are updated at approximately 1 Hz.

Data collection system

To provide data for analysis of navigation performance position and time information is encoded in a standard NMEA string. This string is then broadcast via the serial port. Any device that connects to this serial port then 'sees' a standard GPS device. For initial studies a laptop computer running Navy Personal Flight Planning Software (N-PFPS) was used to display and record aircraft track. The system is currently integrated with the eye-tracking equipment to allow for synchronization of eye-track data (scan pattern) and aircraft track (navigation performance).

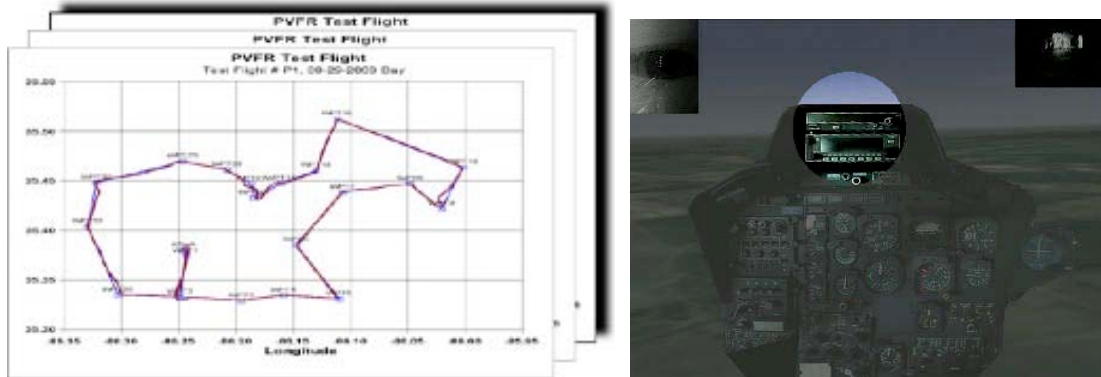


Figure 5. Test flight data (left) and eye tracking system output (right).

Geometric model

The terrain model (Figure 6) was constructed from elevation data, satellite imagery and cultural data using TerraVista 4.0 3D terrain construction software for real-time simulation. The output was a Flight model, with approximately 64 polygons per square kilometer on the Low LOD, and 256 on the High. Data sources: Elevation Data: NIMA DTED Level 1 (100-meter post spacing) was applied to an area of approximately 900 square kilometers. Satellite imagery: The terrain image blends a 1-meter b&w photo (supplied by MapMart, Englewood, CO) with a low-resolution color image. Cultural data: The vectors were hand-built to match visible features in the satellite imagery. Generic features like bridges and overpasses were generated by TerraVista. A number of antennas, power and water towers were hand-modeled from photos of the actual features and placed at their actual locations on the terrain.



Figure 6. A comparison of real to virtual Tullahoma.

PROGRESS ON FLIGHT VIDEO DATA ANALYSES FOR ASSESSMENT OF PVFR ROUTES AND SNI OPERATIONS FOR ROTORCRAFT

Jeffrey B. Mulligan
NASA Ames Research Center, MS 262-2, Moffett Field, CA 94035

Background: In the fall of 2003, a series of flight tests were performed in the Tullahoma, Tennessee area to assess the ability of non-instrument rated helicopter pilots to fly precision routes with the aid of a Global Positioning System (GPS) receiver. During each flight, recordings were made from four video cameras, two of which were attached to a goggle frame worn by the pilot. This paper describes the processing methodologies developed for these data.

INTRODUCTION

This research project seeks to determine the extent to which a cockpit GPS receiver can enable VFR pilots to adhere to precision routes, allowing Simultaneous Non-Interfering (SNI) operations in conjunction with fixed-wing traffic. To this end, a series of flight tests were flown in October 2003, in which pilots flew a route specified by 21 waypoints, some of which corresponded to visible landmarks, and others which were specified only by their latitude and longitude. Complete details of the route and flight test protocol can be found in Hickok & McConkey (2003).

Video data was collected during each flight using the Ames portable eye-tracking system, described in Darken et al. (2003). This system recorded four video streams onto a single 8mm videocassette. Additionally, two audio channels were recorded, one of which consisted of the cockpit audio, while the other channel was used to record video time code and GPS data. The remainder of this paper describes the processing applied to the video data and the current state of the analyses.

VIDEO PROCESSING

Before any processing could be done, the data first had to be transferred from the tapes to a computer. This was done at the University of Tennessee Space Institute (UTSI) campus, using a computer workstation equipped with an analog frame grabber (Matrox Meteor 1). Specially developed software allowed real-time digitization to a pair of dedicated hard disk drives with a capacity of approximately 30 minutes. As each recording had a duration of approximately 1 hour, each recording had to be digitized in two sections. After digitization, the "raw" images were converted to JPEG sequences, and moved to a conventional file system. The audio and GPS recordings were digitized along with the video. Following this procedure, the files

were transferred from UTSI to NASA Ames over the internet.

Camera Demultiplexing

Figure 1 shows a typical video field. Each field consisted of four quadrants, each of which corresponded to one of the four cameras. Camera demultiplexing refers to the process of taking a single movie consisting of the composite frames, and creating four movies corresponding to the individual camera streams. This was accomplished by a straightforward selection of the spatial subregions corresponding to each camera's image. The process was complicated, however, by the fact that the quad processor (which combined the four camera signals into a single signal) sampled the camera signals asynchronously; in other words, each frame put out by the quad processor and captured on tape consisted not of a complete frame from each camera, but was generally made up of portions of two consecutive camera frames. When the objects viewed by the camera were stationary, this could be ignored, but when the objects moved the result was a "tearing" of the frame (see figure 2). Because each of the four cameras had its own clock, the frame rates were all slightly different, and the tearing artifact occurred at a different position within each subimage.

This artifact was eliminated by first locating the occurrence of the tearing artifact, by looking for image discontinuities between pairs of adjacent scan lines. The vertical position within the frame containing the maximum discontinuity was determined, and plotted as a function of time. Because the artifact was produced by the difference in clock frequencies between the two devices, the discontinuities corresponding to the artifact fall on a function which is linear in time, resembling a "sawtooth." We fit a model to the observed data to reject outliers generated by vertical discontinuities in the image not related to the artifact.



Figure 1: Typical raw video field showing images from the four cameras; upper left: over-the-shoulder view from fixed camera; upper right: head-mounted eye camera; lower left: forward-looking head-mounted scene camera; lower right: view of pilot's head from camera fixed to instrument panel.



Figure 2: Recorded eye camera image showing “tearing” artifact resulting from rapid motion of the eye interacting with temporal resampling done by the quad processor. An additional complication arises from the fact that the quad processor uses the interlaced format for its output signal. To reconstruct a camera field, we must “deinterlace” the recorded video from the quad processor. When the tearing artifact is present, it is only visible in one of the two fields output from the quad processor. Depending on whether it is the first or the second field, we must go forward or backward in

time to recover the missing parts of the frame.

Vibration Compensation

In viewing the recordings from the “face camera” mounted on the instrument panel, non-rigid distortions of the image were observed, which were presumed to result from vibration of the camera. These distortions were corrected as follows: first, a few prominent stationary features (parts of the vehicle visible to the sides of the pilot) were identified and tracked over the entire sequence. The motion of the camera in time was recovered from these displacements by remembering that the video lines are scanned sequentially in time; thus, the time at which a feature was imaged was proportional to the vertical position within the frame. After assigning the proper time to each observation, the motion was well-fit by a simple sinusoid. Using the inferred motion of the camera, the images were then warped to produce a relatively undistorted sequence.

Eye Camera Video

Our initial analysis of the eye camera images consisted of localization of the pupil (inner boundary of the iris) and the corneal reflection of the infrared LED's used to illuminate the eye. (In the day flights, the illumination provided by the LED's was generally much less than the ambient illumination, but the reflections of the LEDs themselves were still visible.)

For the night flights, we obtained images similar to those we routinely gather in the laboratory. The images from the day flights, however, posed some new challenges. Because the ambient daylight illumination was much stronger than that provided by the LED illuminators, these sequences are rife with illumination variations, as the vehicle changed its attitude relative to the sun. Another source of illumination variations was the vehicle rotor: because the clear windshield extended back over the pilot's head, a shadow was cast as the rotor passed overhead. Because this was a brief event, it only affected a few video scan lines, producing a dark band in the image (see Figure 3). The band appears vertical in figure 3 because the image has been rotated to put the eye in the proper orientation.



Figure 3: Day flight eye image showing dark band caused by rotor shadow, and partial occlusion of the eye by the upper lashes.

In addition to the illumination variations, there are a number of other features of the daylight eye images which have made robust tracking problematic. Because of the high ambient light levels, the pupil tends to be constricted, making it a smaller target. Similarly, the resting pose of the eyelids tends to be more closed, as if the pilots were squinting. This is problematic for two reasons: first, the eyelids hide more of the eye when they are partially closed; second, the upper eyelashes move in front of the pupil as the lid is closed, obscuring the features we are trying to detect.

Because of all these factors, our initial efforts to track the eye in the daylight videos have been only partially successful, with estimates obtained for only about 40% of the frames in the two flights processed. To overcome this shortcoming, we plan to redo the analysis, introducing a number of new techniques. In frames where the eye is visible, we will track the limbus (outer margin of the iris) in addition to the pupil. In addition to providing an additional feature, localization of the limbus will also provide a check on the pupil localization, because these two features should share a common center. (Refraction by the cornea makes them have slightly different centers for eccentric gaze directions, but this can be taken into account.)

We also plan to introduce methods to estimate gaze direction when the eye itself is hidden by the upper eyelid. We expect that the vertical component of gaze will be especially easy to recover, because the lid

moves with the eye, and therefore the vertical position of the lid is monotonically related to the vertical component of gaze. The horizontal component may be more difficult to extract, but we note that because of the fact that the cornea is a small dome rising out of the roughly spherical eyeball, its lateral motion causes a change in the shape of the covering eyelid, and in particular the form of the margin of the lid. Accuracy using this technique may suffer for two reasons: first, the measure itself is likely to be less sensitive than direct measurement of the pupil position; and second, we may not have calibration data for the extreme down-gaze positions for which the lid entirely hides the eye. However, these gaze directions do not correspond to those of most interest for this study (i.e., the GPS receiver and out-the-window landmarks), but rather correspond to the instruments at the bottom of the panel, and charts in the pilot's lap. Therefore, we believe that degraded accuracy for these gaze targets will be acceptable.

Face Camera Processing

We obtain an estimate of the pose of the pilot's head by analysis of the images from the fixed camera mounted on the instrument panel. Our procedure is a mix of automatic and manual procedures. First, a set of conspicuous features on the head are selected, such as the headset earphones, the microphone, etc. Next, a training set of 150 frames is selected. For each frame in the training set, an operator manually indicates the position of each feature using the mouse.

At this point, we have 150 views of each feature, stored as small subimages. The various appearances of a feature can be efficiently described using a small number of parameters by applying a Principal Components Analysis (PCA) to the set of feature appearances, a technique first applied to entire face images by Turk and Pentland (1991).

We next obtain an approximate 3-dimensional configuration of the features from a pair of "mug-shot" views, that is by picking a view which is close to frontal and another which is nearly profile. The positions of the features in the frontal view give us the approximate x (side-to-side) and y (vertical) coordinates of the features, while the profile view provides approximate z (fore-and-aft) and y . We then refine the the estimates by alternately optimizing the structure and pose parameters over all 150 training images. This procedure stabilizes after 2 or 3 iterations, at which point we have estimates of both the 3-D structure of the features, and the pose of the head in each of the training images.

The next step is to derive the relationship between the pose and the appearance of each of the features (as described by the eigen-feature coefficients). For each

training frame, we have a set of pose parameters (angles) and a set of coefficients describing the appearance of the features. We derive an algebraic relation between the pose angles and each of the coefficients, which allows us to predict the appearance of each feature for an arbitrary pose – including poses which we may not have seen before.

We are now ready to describe the pose estimation process for an arbitrary new frame: we first make a guess about the pose, either recycling the final pose estimate from the previous frame, or assuming a frontal view for the first frame. Using this guess, we predict the corresponding appearance of each of the features. Using the expected feature appearances, we then search for each of the features in the image using cross-correlation. From the locations of the features, we estimate the pose. If the new estimate of the pose differs from our initial guess, we recompute the appearance of the features using the new pose estimate, and repeat the process until the estimate is stable (usually 2-3 iterations). Typical results are shown in figure 5.



Figure 5: Face camera image with line overlaid rendering of 3-D line segment model linking feature points.

Scene Camera Processing

The images gathered by the head-mounted scene camera provide a second source of information about the position and orientation of the head. *Structure-from-motion* refers to a technique by which both the camera pose and the 3-D locations of scene features can be computed from a series of images. While we ultimately hope to apply this technique, here we present a simpler method in which we approximate the camera motion by a pure rotation about the camera's optical nodal point. This simplification affords two advantages: first, we do not have to solve for the 3-D structure (or construct an accurate model of the cockpit interior); second, instead of identifying and tracking individual features, we can simply solve for the camera

pose parameters which provide the best overall registration of the image with the previous image or a template formed by mosaicing a set of images.

To register images related by large rotations, we must take into account the effect of the perspective projection performed by the camera-lens system. Because the camera-lens system projects the sphere of viewing directions onto a flat image plane, it is necessary to apply a complex non-rigid warp to bring two images into correspondence. We address this problem by adopting a cylindrical coordinate system to which we transform all the images.

To derive the transformation from the image sensor coordinates to the global coordinate system, we assume a generic pinhole camera model. But this is a poor approximation to our actual camera, which has a short focal length wide-angle lens which introduces considerable lens distortion. This distortion is evident in the appearance of the horizon, which usually appears curved in the raw video images. We apply an approximate correction for lens distortion by assuming a generic lens distortion model, and adjusting its single parameter to produce a linear horizon in a small number of representative frames.

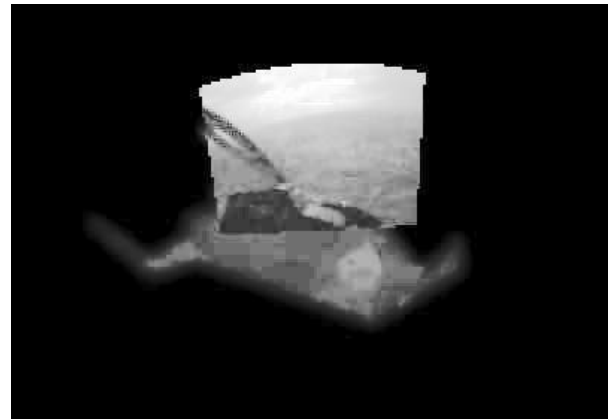


Figure 6: Composite image showing image from scene camera warped to cylindrical coordinate space, and overlaid on mosaic of instrument panel.

After correcting the raw video for lens distortion, we proceed to construct a mosaic of the cockpit as follows: we initialize the mosaic using an image filled by the instrument panel. Successive images are processed by first making an initial guess concerning the camera orientation (usually the orientation estimated for the previous frame). We then use the estimated orientation to warp the image to the common image space. The quality of the resulting registration is assessed by computing the normalized cross-correlation. The STEPIT optimization routine (Chandler, 1969) is used

to adjust the rotation parameters to optimize the fit.

Typical images from the scene camera contain both fixed features of the cockpit, and moving terrain features seen out the window. Because of the motion of the aircraft, these terrain features are not useful in determining the pose of the head, and we therefore wish to exclude them from the registration process. This is done by hand-construction of a mask which selects the portion of the mosaic image corresponding to the vehicle instrument panel and frame. Figure 6 shows the masked mosaic, with an input frame registered and overlaid.

SUMMARY

We have described a number of image processing procedures which have been applied to video data collected in the 2003 Tullahoma data collection flights. Our most reliable data has been obtained from the face-camera-based head pose estimation, with estimates obtained for approximately 85% of all frames, while the least reliable has been the day flight eye camera measurements, with estimates obtained for only 40% of all frames. We hope to improve the reliability and accuracy of all measures in the coming year.

REFERENCES

Chandler, J. P. (1969). "Subroutine STEPIT – Finds local minima of a smooth function of several parameters," *Behavioral Science*, v. 14, pp. 81-82.

Darken, R. P., Sullivan, J. A., and Mulligan, J. B. (2003). "Progress on the simulator and eye-tracker for assessment of PVFR routes and SNI operations for rotorcraft," FAA FY03 program review, Human Factors Vertical Flight.

Hickok, S. M., and McConkey, E. D. (2003). "Flight test plan to assess of PVFR routes and SNI operations for rotorcraft," FAA FY03 program review, Human Factors Vertical Flight.

Turk, M., and Pentland, A. (1991). "Eigenfaces for recognition," *Journal of Cognitive Neuroscience*, v. 3(1), pp. 71-86.

NIGHT VISION IMAGING SYSTEM LIGHTING COMPATIBILITY ASSESSMENT METHODOLOGY: PART 2

*H. Lee Task, Ph.D., §Alan R. Pinkus, Ph.D., †Maryann H. Barbato, †Martha A. Hausmann
*Task Consulting, Dayton, Ohio
§Air Force Research Laboratory, Wright-Patterson AFB, Ohio
†General Dynamics, Inc., Dayton, Ohio

If night vision goggles (NVGs) are to be safely used by pilots, it is necessary that the cockpit lighting and displays be compatible with the operation of the NVGs. The current standard field practice for verifying that cockpit lighting and displays are compatible with the NVGs is to conduct a visual acuity degradation assessment. This method is subjective and, as the research described herein, relatively imprecise. An alternative method is to directly measure the amount of interfering light caused by the cockpit lighting and displays. This is referred to as the NVG light output method or NLO. The research reported here demonstrates the superiority of the NLO method compared to the visual acuity method with respect to objectivity and precision. Although the NLO method still needs some further refinement, it is recommended that this method be adopted as a standard field method for assessing cockpit lighting compatibility.

INTRODUCTION

The study and results described in this document are a follow-on effort to a study that was previously reported¹⁰. Much of the fundamental introductory material will not be repeated here. Therefore, it is recommended that this report be read in conjunction with reference 10 if the reader is unfamiliar with the basic issues being addressed in this study. Prior work¹⁰ has established the viability of an inexpensive, alternative method of determining whether or not a cockpit lighting system is compatible with the operation of night vision imaging systems (NVIS) such as the night vision goggles (NVGs) shown in Figure 1.

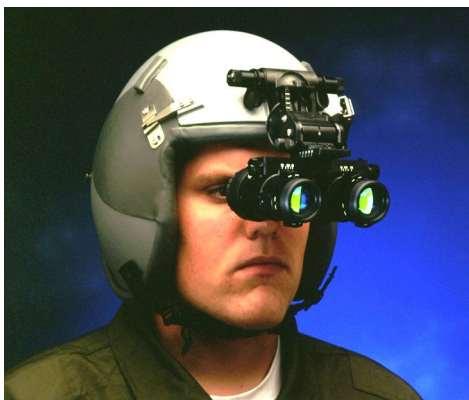


Figure 1. F4949 night vision goggles

Unmodified aircraft cockpit lighting and displays can interfere with the proper operation of NVGs in several specific ways. For each interference mechanism, the effect on the image seen through the NVGs is a reduction of the light level or contrast of the view outside the aircraft. This reduction in light level or contrast can be manifested as a reduction in visual acuity and/or as an observed loss of contrast or brightness. Many techniques have been developed to produce cockpit lighting and displays that are reasonably compatible with the operation of NVGs¹. *Reasonably compatible* means there is sufficient light for the pilot to view his/her instruments and displays (note: pilots look *under* the NVGs to directly view their instruments) but the lighting is such that it does not significantly interfere with the image of the exterior scene viewed through the NVGs.

Phase 1 of this joint research effort¹⁰ between the Federal Aviation Administration (FAA) and the US Air Force Research Laboratory (AFRL/HECV) investigated the visual acuity assessment method using inexpensive equipment as well as an objective method based on NVG light output. The results from this first phase demonstrated that the visual acuity assessment method could be conducted just as well with inexpensive equipment and that the visual acuity method was relatively imprecise when compared to the inexpensive, objective method. The

objective method investigated was based on measuring the relative amount of light output increase that was encountered as the cockpit lighting and displays were turned “on” compared to the “off” condition. This extra light output is what would cause interference in the NVGs and thus should be related to the degradation in image quality of the NVG image. For simplicity, this objective method will be referred to as the NVG light output method or NLO method.

Although the results of the first phase of this joint effort were quite encouraging regarding the use of inexpensive equipment for assessing NVIS lighting compatibility for both the visual acuity (VA) and the NLO methods, there were three issues that needed to be resolved. The first issue related to the basic method of the study. In this first study, subjects viewed the visual acuity chart through the NVGs for six different NVIS radiance levels, plus lights off. These seven levels were presented randomly to make the study more objective. The current practice in the field is to look at the VA chart with lights “off” immediately followed by lights “on” to make it easier to compare the two conditions. Therefore the first study did not exactly duplicate what is currently done in the field, but rather used a procedure that was slightly more objective.

The second issue deals with the NLO method. This method uses an inexpensive illuminance meter taped to the eyepiece lens of the NVG so that a light reading is obtained that is proportional to the average scene luminance of the NVG image. Subjects were instructed to point the NVGs with the attached light meter through the simulated windscreen just as if they were looking through the NVGs at the visual acuity chart; only the illuminator for the VA chart was not on. Since there was no precision in pointing the NVGs through the simulated windscreen, it was possible that some of the field of view of the NVGs could contain the image of the cockpit lighting simulator, which could lead to a higher amount of variance in the NLO readings for the same NVIS radiance conditions.

The third issue has to do with selecting a “compatibility cut-off” level for the NLO method. Because of the relatively low light output level of the NVGs, the diffuser on the illuminance meter had to be removed to provide increased sensitivity. This means the light output

is not calibrated to any specific, accepted photometric units. Since NVGs can vary in their maximum light output and in their gain values, some type of relative value (relative to the specific NVG used) must be established for acceptance/rejection criteria.

Resolving these three issues was the primary goal of the current research reported in this document. Issue one was addressed by presenting subjects with consecutive “off” then “on” conditions to accurately simulate the current field method. For issue two, subjects were instructed to look through the other ocular of the NVGs and make sure that no part of the cockpit lighting simulator that was emitting light was within the field of view of the NVGs. The third issue was resolved by determining the light meter reading when the NVGs were at their maximum output luminance. Then the criteria level would be a fixed fraction of this maximum light output level (e.g., 1% or ½%). This would insure that the amount of interfering light is a small fraction of the total NVG image light. This value was selected *ex post facto* to correspond to some other currently accepted criteria level dealing with visual acuity loss or NVIS radiance level. This is explained more fully in the analysis and discussion sections.

As in Phase 1, the primary results of this study are a collection of “probability of rejection” curves that graph the probability of rejecting the lighting system, because it is incompatible, against the NVIS radiance level.

APPROACH

The currently accepted visual acuity-based NVIS lighting evaluation method (henceforth called the “VA baseline method”) was the baseline for this study. In order to determine if the NLO method was as good as the VA baseline method, some means needed to be devised to characterize the *goodness* of these methods so that they can be compared. Since the primary objective of doing an NVIS lighting evaluation is to make a pass/fail determination as to the compatibility of the NVIS lighting, it was possible to develop a probability of rejection (i.e., failure) of the lighting system as a function of the NVIS lighting radiance level, which is the basic criteria stated in the military specifications. For each NVIS radiance level, the

study provided repeated measures of “accept” or “reject” for each subject and the two evaluation methods. These repeated measures could be directly converted to a probability of pass or fail and graphed against the NVIS radiance level, thus producing the probability of rejection curve. Ideally, one would like this curve to be flat at 0% from an NVIS radiance level of zero out to some NVIS radiance level which marks the boundary between acceptable and unacceptable, and then the curve would shoot up to 100% just past that critical NVIS radiance level. If the curve gradually increases as a function of NVIS radiance then it indicates the method is relatively imprecise and prone to Type I and Type II errors (rejecting something that should have been accepted and accepting something that should have been rejected). Therefore the slope of the probability of rejection curve at the 50% probability point can be used as a measure of the precision of the evaluation method, one measure of the *goodness* of the method.

Two basic interference conditions were investigated: 1) light was reflected in the windscreen and 2) light was blocked from reflecting in the windscreen. The first condition causes a veiling luminance from the reflection and the second condition may cause a veiling luminance from light scatter within the objective lens of the NVGs. A total of six NVIS radiance levels were used for each of the two interference conditions (the levels were different for the two conditions because it required much more NVIS radiance to induce interference in the non-reflected mode versus the reflected mode). Each subject was presented with 10 trials for each NVIS radiance level, condition, and evaluation method. A trial consisted of a baseline measurement (either visual acuity or NVG light output) with the simulated cockpit lighting “off” and then a test measurement with the simulated cockpit lighting “on.” This resulted in a total of 120 data points per subject (10 trials, six radiance levels, two interference conditions).

METHOD

Subjects: Three males and three females, ranging in age from 40-53, participated in this study. Prior to participation in the study, all observers underwent a visual examination to

insure they had normal or corrected acuity of 20/20 or better.

Apparatus: A basic cockpit lighting simulator (NVIS lighting simulator or NLS) was used to recreate the lighting interference conditions and the aircraft windscreen and glare shield. The USAF 1951 Tri-bar chart was used to measure visual acuity, and was illuminated using a calibrated incandescent lamp. The NVIS radiance on the chart was monitored using a Photo Research 1530AR radiometer. Model F4949C NVGs were used in this study. An Extech Light ProbeMeter was attached to the NVGs to measure the luminance output of the goggles. The actual radiance and luminance of the lighting simulator was measured using an Instrument Systems Model 320 spectral scanning radiometer. For this study, the lighting simulator was configured in either a reflected or non-reflected mode.

Procedure: Subjects were seated behind the NLS and the armrest and seat height were adjusted. Since the NVGs were hand held, the armrest was positioned to allow proper alignment with the stimulus and to reduce fatigue. The room lights were turned off and the subject dark-adapted for 12 minutes. The subjects were then asked to focus the NVGs. For the reflected and non-reflected conditions, the following two tasks were counterbalanced. The NVIS radiance light levels were randomly presented for each task.

Task 1: With the NVIS lighting “off,” subjects looked through a pair of F4949C NVGs at the Tri-bar chart and identified the group and element number of the smallest set of horizontal and vertical bars they could resolve. The lighting was then turn “on” and the subjects determined if there was a change in the group and element number they could resolve. Subjects closed their eyes between trials while the experimenter adjusted the NVIS radiance of the NLS.

Task 2: An Extech Light ProbeMeter was taped to the eyepiece of the right ocular of the NVGs using black masking tape. With the NVIS lighting in the “off” position, subjects viewed through the left ocular of the NVGs to aim the NVGs through the windscreen. The experimenter recorded this baseline reading then switched the NVIS lighting “on” and recorded the baseline plus interference reading. NVIS

radiance conditions were presented in a randomized order.

RESULTS

Although the individual subject data are of extreme interest due to some individual differences, there is insufficient space in this report to include those data. Figures 2 and 3 show the composite probability of rejection curves for all six subjects for the VA baseline method and the NLO method, respectively, for each of the two interference conditions (reflected mode and non-reflected mode). The graphs shown in Figures 2 and 3, depict the slopes of the curves at the 50% probability level and are summarized in Table 1.

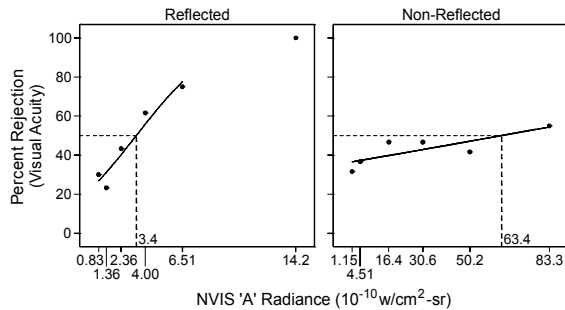


Figure 2. Probability of rejection curves for the VA baseline method for all six subjects combined. The dashed line corresponds to the 50% probability level. Each data point is the average over 60 samples (Six subjects, 10 trials each).

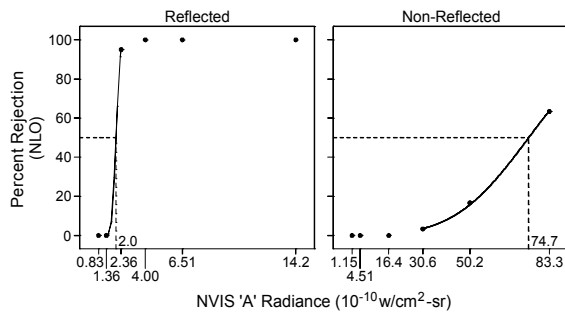


Figure 3. Probability of rejection curves for the NLO method for all six subjects combined. The dashed line corresponds to the 50% probability level. Each data point is the average over 60 samples (Six subjects, 10 trials each).

Table 1. Slopes of the probability of rejection curves at the 50% probability point. Values represent change in percent rejection for a 1 unit ($10^{-10} \text{w/cm}^2\text{-sr}$) increase in radiance. The higher the number the more precise the method (less chance of a Type I or Type II error).

Reflected	Visual Acuity	NLO
Yes	9.64	189
No	0.22	1.64

DISCUSSION AND CONCLUSIONS

The visual acuity results of this study, as depicted in Figure 2, are somewhat different than the previous study¹⁰. The slopes of the reflected mode rejection curves for the two studies are similar but the 50% rejection NVIS radiance point has been shifted by about 50 percent. The reflected mode shifted from a 50% rejection point NVIS radiance of 2.1 in the previous study (after NVIS radiance values of the previous study were corrected) to a 3.4 in the current study. However, the non-reflected mode visual acuity rejection curve did not change by much, shifting from 71.2 in the previous study to 63.4 in this study. The shift in the reflected mode 50% rejection point radiance may indicate that the first issue as discussed in the Introduction Section, regarding having an “off” condition always immediately preceding the “on” condition, did have an effect on the visual acuity “leniency” in allowing a lighting system to pass. From the results, using the 50% criteria point, the current field evaluation method is 50% more lenient (allowing lighting systems with higher NVIS radiance values to pass) as the more objective visual technique that was used in Phase 1.

The most striking results of this study, as in the first study, are apparent from Figures 2 and 3 and Table 1. The NLO method produces a much steeper probability of rejection curve, which means this method is much more precise than the visual acuity method. The technique of making sure the NVIS lighting was not in the field of view of the NVGs (for the non-reflected mode) had a substantial impact on the NLO method results in that it shifted the 50% probability point NVIS radiance from 5.9 in the previous study to 74.7 in this study, which is more in concert with the relatively aimless visual acuity results for the

non-reflected mode. This answers the question regarding issue two, described in the Introduction Section, where the NVIS lighting had an unintended affect on the NLO method if it was within the field of view.

The criteria value (what light level reading to use as the demarcation between acceptable and unacceptable lighting) was explored a little bit in this study. The curves shown in Figure 3 used a cut-off value of 0.148 (reading on the light meter), which corresponded to 1/2% of the maximum light output reading for that NVG. This is a very conservative value and should be investigated in future research.

The main conclusion from these studies is that the NLO method appears to be a very promising objective method of assessing the compatibility of cockpit lighting systems with NVGs. It can be used as a supplement to the visual acuity method or can easily be used to replace the visual acuity method. However, it should be required that a visual inspection of the lighting system, for reflections at particularly objectionable locations, and for light leaks, be performed using NVGs. Another fact that is evident from these studies is the considerable imprecision of the visual acuity method and its corresponding susceptibility to Type I and Type II errors (rejecting a lighting system that should have been accepted and accepting a lighting system that should have been rejected).

It is recommended that the NVG light output method be adopted as a standard, objective method of verifying that the cockpit lighting and displays are compatible with the operation of the NVGs.

REFERENCES

1. RTCA/DO-275, 12 October 2001. *Minimum operational performance standards for integrated night vision imaging system equipment*, prepared by SC-196, Washington, DC.
2. Task, H. L., & Griffin, L. L. (1982). PAVE LOW III: Interior lighting reconfiguration for night lighting and night vision goggle compatibility. *Aviation, Space & Environmental Medicine*, 53, 1162-1165.
3. ASC/ENFC 96-01 REV 1, 22 March 1996. Interface document, lighting, aircraft, interior, Night Vision Imaging System (NVIS) compatible. Wright-Patterson AFB, OH: ASC ENFC.
4. MIL-STD-3009, 2 February 2001. *Dept of Defense interface standard for lighting, aircraft, Night Vision Imaging System (NVIS) compatible*.
5. MIL-L-85762A, 26 August 1988. *Military specification, lighting, aircraft, Night Vision Imaging System (NVIS) compatible*.
6. Reising, J. D., Antonio, J. C., & Fields, B. (1995). *Procedures for conducting a field evaluation of night vision goggle-compatible cockpit lighting*. (Report No. AL/HR-TR-1995-0167).
7. Reetz III, F. (1987). *Rationale behind the requirements contained in military specs MIL-L-85762 and MIL-L-85762A*. (Technical Report NADC-87060-20). Warminster, PA: Naval Air Development Center.
8. Interagency Agreement DTFA01-02-X-02017 (February 2002) between the Federal Aviation Administration (FAA) and the Department of Defense Air Force Research Laboratory (AFRL/HEC, Wright-Patterson AFB).
9. Finney, D. J. (1980). *Probit analysis* (3rd ed.). Cambridge: Cambridge University Press.
10. Task, H. L., Pinkus, A. R., Barbato, M. H., and Hausmann, M. A. (2003). Night vision imaging system lighting compatibility assessment methodology. *Human Factors Vertical Flight Program Review FY03*, FAA AAR-100, Washington D. C.

ACKNOWLEDGEMENTS

The authors gratefully acknowledge the excellent technical support of Sheldon Unger and David Sivert of General Dynamics, Inc., Dayton, OH.